

## Spectroscopic and Structural Study of Metal–Metal Bonded Metalloporphyrinic Derivatives: the Case of Rhodium–Indium

D. Daphnomili,<sup>†</sup> C. Raptopoulou,<sup>||</sup> A. Terzis,<sup>||</sup> J.-H. Agondanou,<sup>‡</sup> S. Bénazeth,<sup>‡,§</sup> and A. G. Coutsolelos<sup>\*,†</sup>

Laboratory of Bioinorganic Coordination Chemistry, Department of Chemistry, School of Sciences, University of Crete, P.O. Box 1470, 71409 Heraklion Crete, Greece, Laboratoire de biomathématiques, Faculté de pharmacie Université Paris V, 4 avenue de l'observatoire, 75006 Paris, France, LURE, Bat 209D, Université Paris XI, 91405 Orsay, France, and NCRS, Demokritos, Agia Paraskevi, 15310 Athens, Greece

Received October 6, 2003

The synthesis and spectroscopic characterization of heterometallic porphyrinate derivatives containing rhodium–indium metal–metal bonds are reported. The investigated compounds are represented by the formula [(Porph)-RhIn(Porph')], where Porph and Porph' are OEP, TPP,  $\beta$ -Cl<sub>4</sub>TPP,  $\beta$ -Cl<sub>8</sub>TPP, or TPyP. UV–Visible spectroscopy of the title complexes confirms the presence of a strong  $\pi$ – $\pi$  interaction between the macrocycles in each derivative and denotes the effect of the nontransition metal in their optical features. For comparison purposes, a new bimetallic complex with a rhodium–thallium metal–metal bond is also presented. According to <sup>1</sup>H and <sup>13</sup>C NMR data, we were able to distinguish two major NMR regions: the *endo*- between the metal–metal bonded macrocycles and the *exo*-, which are characteristic features of porphyrinic complexes at very close proximity. X-ray absorption spectroscopy (XAS) structural characterization of Rh–In bond was performed on the [(OEP)RhIn(OEP)] complex, in the fluorescence mode, and we essentially focused on the metal–metal distance determination. Finally, the distance of 2.543(3) Å was deduced from the X-ray structure of a new [(TPP)RhIn(TPyP)] derivative.

### Introduction

The majority of the metal–metal bonded porphyrinic derivatives possess multiple M–M bonds<sup>1–19</sup> in contrast to those with single bonds. The only known porphyrinic

complexes with single bonds are those with Rh<sup>20,21</sup> or Ir,<sup>22</sup> which exhibit catalytic activities.<sup>23–26</sup> A main reason for this was the lack of easily prepared heterometallic derivatives in analytically pure form. Because our studies are focused on this field, we have been able to elucidate a synthetic procedure for the quantitative preparation of single metal–

\* Author to whom correspondence should be addressed. Phone: +30.2810.393636. Fax: +30.2810.393601. E-mail: coutsole@chemistry.uoc.gr.

<sup>†</sup> University of Crete.

<sup>||</sup> Faculté de pharmacie Université Paris V.

<sup>§</sup> LURE, Université Paris XI.

<sup>¶</sup> NCRS.

- (1) Collman, J. P.; Arnold, H. J. *Acc. Chem. Res.* **1993**, 26, 586.
- (2) (a) Collman, J. P.; Woo, L. K. *Proc. Natl. Acad. Sci., U.S.A.* **1984**, 81, 259. (b) Collman, J. P.; Arnold, H. J.; Fitzgerald, J. P.; Weissman, K. J. *J. Am. Chem. Soc.* **1993**, 115, 9309.
- (3) Collman, J. P.; Garner, J. M. *J. Am. Chem. Soc.* **1990**, 112, 166.
- (4) Collman, J. P.; Barnes, C. E.; Collins, T. J.; Brothers, P. J.; Callucci, J.; Ibers, J. I. *J. Am. Chem. Soc.* **1981**, 103, 7030.
- (5) Collman, J. P.; Barnes, C. E.; Woo, L. K. *J. Am. Chem. Soc.* **1989**, 111, 8141.
- (6) Collman, J. P.; Barnes, C. E.; Swepston, P. N.; Ibers, J. A. *J. Am. Chem. Soc.* **1984**, 106, 3500.
- (7) Collman, J. P.; Kim, K.; Garner, J. M. *J. Chem. Soc., Chem. Commun.* **1986**, 1711.
- (8) Collman, J. P.; Arnold, H. J.; Weissman, K. J.; Burton, J. M. *J. Am. Chem. Soc.* **1994**, 116, 9761.
- (9) Collman, J. P.; Fish, H. T. *Inorg. Chem.* **1996**, 35, 7922.

- (10) Collman, J. P.; Garner, J. M.; Hembre, R. T.; Ha, J. *J. Am. Chem. Soc.* **1992**, 114, 1292.
- (11) Kim, J. C.; Goedken, V. L.; Lee, B. M. *Polyhedron* **1996**, 15, 1, 57.
- (12) Collman, J. P.; Prodollet, J. W.; Leidner, C. R. *J. Am. Chem. Soc.* **1986**, 108, 2916.
- (13) Tait, C. D.; Garner, J. M.; Collman, J. P.; Sattleberger, A. P.; Woodruff, W. H. *J. Am. Chem. Soc.* **1989**, 111, 7806.
- (14) Tait, C. D.; Garner, J. M.; Collman, J. P.; Sattleberger, A. P.; Woodruff, W. H. *J. Am. Chem. Soc.* **1989**, 111, 9072.
- (15) Yang, C. H.; Dzugan, S. I.; Goedken, V. L. *J. Chem. Soc., Chem. Commun.* **1986**, 1313.
- (16) Collman, J. P.; Harford, S. T.; Maldivi, P.; Marchon, J. C. *J. Am. Chem. Soc.* **1998**, 120, 7999.
- (17) Collman, J. P.; Harford, S. T. *Inorg. Chem.* **1998**, 37, 4152.
- (18) Collman, J. P.; Harford, S. T.; Franzen, S.; Marchon, J. C.; Maldivi, P.; Shreve, A. P.; Woodruff, W. H. *Inorg. Chem.* **1999**, 38, 2085.
- (19) Collman, J. P.; Harford, S. T.; Franzen, S.; Shreve, A. P.; Woodruff, W. H. *Inorg. Chem.* **1999**, 38, 2093.
- (20) Setsune, J. I.; Yoshida, Z.-J. *J. Chem. Soc., Perkin Trans. I* **1982**, 983.

metal bonded derivatives between a transition and a non-transition metalloporphyrin.<sup>27,28</sup>

Continuing our effort of probing the nature of the single metal–metal bond, we report herein the synthesis and the physicochemical characterization of a new series of derivatives with Rh–In metal bond. One of our research objectives has been the elucidation of the contribution of steric and electronic properties of the porphyrinic ligands to the formation of the dimetallic bond. For this purpose,  $\beta$ -halogenated and *meso*-substituted porphyrins are used as the four-coordinated ligands of the nontransition metal. The physicochemical properties of the formed complexes are discussed in terms of their optical features and NMR data. For comparison purposes, a new complex with Rh–Tl bond, [(OEP)RhTl( $\beta$ -Cl<sub>8</sub>TPP)], is also reported.

As far as structural data are concerned, an EXAFS structural approach focused on the dimetallic distance determination of [(OEP)RhIn(OEP)] is presented, which provides information on the stability of the complex. Finally, the X-ray structure of [(TPP)RhIn(TPyP)] is presented.

## Experimental Section

**Materials.** All chemicals were reagent grade and were used without further purification, except as noted. Basic type I alumina was activated at 150 °C for a minimum of 24 h. THF and toluene were distilled over sodium/benzophenone under an inert atmosphere. Ethanol and the basic aqueous solution (0.5 M) of NaBH<sub>4</sub> were degassed via three freeze–pump–thaw cycles. Manipulation of oxygen-sensitive compounds (reduced Rh(I) porphyrinic species with OEP or TPP and preparation reactions for the complexes) was carried out on a vacuum line under an argon atmosphere using Schlenk tube techniques. All manipulations of light-sensitive derivatives were carried out in the darkroom (metal–metal bonded derivatives).

**Physical Measurements.** <sup>1</sup>H and <sup>13</sup>C NMR spectra were recorded on a Bruker AMX-500 MHz NMR spectrometer, using chloroform-D<sub>3</sub> as a solvent. Resonances in the <sup>1</sup>H NMR were referenced versus the residual proton signal of the solvent.

Absorption spectra were collected on a Perkin-Elmer Lamda 6 grating spectrophotometer.

- (21) (a) Wayland, B. B.; Newman, A. R. *Inorg. Chem.* **1981**, *29*, 3093. (b) Hoshino, M.; Yasufuka, K.; Konishi, S.; Imamura, M. *Inorg. Chem.* **1984**, *23*, 1982. (c) Del Rossi, K. J.; Wayland, B. B. *J. Chem. Soc.* **1986**, 1653. (d) Ni, Y.; Fitzgerald, J. P.; Carroll, P.; Wayland, B. B. *Inorg. Chem.* **1994**, *33*, 2029. (e) Collman, J. P.; Ha, Y.; Guilard, R.; Lopez, M. A. *Inorg. Chem.* **1993**, *32*, 1788. (f) Feng, M.; Chan, K. S. *J. Organomet. Chem.* **1999**, *584*, 235.
- (22) Chan K. S.; Leung, Y. B. *Inorg. Chem.* **1994**, *33*, 3187.
- (23) Wayland, B. B.; Woods, B. A. Pierce, R. *J. Am. Chem. Soc.* **1982**, *104*, 302.
- (24) (a) Wayland, B. B.; Sherry, A. E.; Poszmiik, G.; Bunn, A. G. *J. Am. Chem. Soc.* **1992**, *114*, 1673. (b) Coffin, V. L.; Brennen, W.; Wayland, B. B. *J. Am. Chem. Soc.* **1988**, *110*, 6063. (c) Wayland, B. B.; Woodsand, B. A.; Coffin, V. L. *Organometallics* **1986**, *5*, 1059.
- (25) (a) Wayland, B. B.; Ba, S.; Sherry, A. E. *J. Am. Chem. Soc.* **1991**, *113*, 5305. (b) Sherry, A. E.; Wayland, B. B. *J. Am. Chem. Soc.* **1990**, *112*, 1259.
- (26) Del Rossi, K. J.; Zhang, X. X.; Wayland, B. B. *J. Organomet. Chem.* **1995**, *504*, 47.
- (27) (a) Coutsolelos, A. G.; Lux, D.; Mikros, E. *Polyhedron* **1996**, *15*, 4, 715. (b) Lux, D.; Daphnomili, D.; Coutsolelos, A. G. *Polyhedron* **1994**, *13*, 2367
- (28) Daphnomili, D.; Scheidt, W. R.; Zajicek, J.; Coutsolelos, A. G. *Inorg. Chem.* **1998**, *37*, 3675.

Crystals of [(OEP)RhIn(TPyP)] derivative suitable for X-ray diffraction were obtained by slow evaporation of a saturated toluene/MeOH solution.

**Synthesis of [(Porph)M<sup>III</sup>Cl].** (Porph)Rh<sup>III</sup>Cl,<sup>29</sup> (Porph)In<sup>III</sup>Cl,<sup>30a</sup> and (Porph)Tl<sup>III</sup>Cl<sup>30a</sup> were prepared according to literature methods.

**Synthesis of [(Porph)Rh<sup>I</sup>]<sup>–</sup>Na<sup>+</sup>.** The reduced species [(OEP)Rh<sup>I</sup>]<sup>–</sup>Na<sup>+</sup> and [(TPP)Rh<sup>I</sup>]<sup>–</sup>Na<sup>+</sup> were prepared according to a previously published procedure.<sup>28</sup>

**Synthesis of [(OEP)RhIn(TPyP)].** (TPyP)In<sup>III</sup>Cl (0.06 mmol) was dissolved under an argon atmosphere in 30 mL of THF. The solution was transferred to the solid residue of [(OEP)Rh<sup>I</sup>]<sup>–</sup>Na<sup>+</sup>. The reaction mixture was stirred at room temperature for 3 h. The solvent was evaporated and the crude product was chromatographed on an Al<sub>2</sub>O<sub>3</sub> column (4 × 3 cm, type I Basic). The porphyrinic derivative was eluted with CH<sub>2</sub>Cl<sub>2</sub>/MeOH (100:0.4 v/v) [yield 30% based on (OEP)Rh<sup>III</sup>Cl].

**Synthesis of [(TPP)RhIn(TPyP)].** (TPyP)In<sup>III</sup>Cl (0.09 mmol) was added in 30 mL of THF under an argon atmosphere. The solution was transferred to the solid residue of [(TPP)Rh<sup>I</sup>]<sup>–</sup>Na<sup>+</sup>. The reaction mixture was stirred at room temperature for 2 h and then evaporated to dryness under vacuum. Pure product was obtained by column chromatography (Al<sub>2</sub>O<sub>3</sub> column, 4 × 3 cm, type I Basic). The porphyrinic derivative was eluted with CH<sub>2</sub>Cl<sub>2</sub>/MeOH (100:0.2 v/v) [yield 25% based on (TPP)Rh<sup>III</sup>Cl]. Dark red crystals suitable for X-ray diffraction studies were obtained by a slow evaporation in the dark of a saturated solution [toluene/MeOH (10:0.1 v/v)].

**Synthesis of [(OEP)RhIn( $\beta$ -Cl<sub>8</sub>TPP)].** ( $\beta$ -Cl<sub>8</sub>TPP)In<sup>III</sup>Cl (0.03 mmol) was dissolved under an argon atmosphere in 30 mL of THF. The solution was transferred to the solid residue of [(OEP)Rh<sup>I</sup>]<sup>–</sup>Na<sup>+</sup>. The reaction mixture was stirred at room temperature for 2 h. After the removal of the solvent, the crude product was chromatographed on an Al<sub>2</sub>O<sub>3</sub> column (6 × 2 cm, type I Basic). The porphyrinic derivative was eluted with a mixture of solvents toluene/hexane (7:3 v/v) [yield 35% based on (OEP)Rh<sup>III</sup>Cl].

**Synthesis of [(TPP)RhIn( $\beta$ -Cl<sub>8</sub>TPP)].** ( $\beta$ -Cl<sub>8</sub>TPP)In<sup>III</sup>Cl (0.04 mmol) was dissolved in 30 mL of THF under an argon atmosphere. The solution was transferred to the solid residue of [(OEP)Rh<sup>I</sup>]<sup>–</sup>Na<sup>+</sup>. The reaction mixture was stirred at room temperature for 2 h. The solvent was evaporated and the crude product was passed through an Al<sub>2</sub>O<sub>3</sub> column (6 × 2 cm, type I Basic). The porphyrinic derivative was eluted with toluene/hexane (8:2 v/v) [yield 20% based on (OEP)Rh<sup>III</sup>Cl].

**Synthesis of [(OEP)RhIn( $\beta$ -Cl<sub>4</sub>TPP)].** ( $\beta$ -Cl<sub>4</sub>TPP)In<sup>III</sup>Cl (0.03 mmol) was added into 30 mL of THF under an argon atmosphere. The solution was added to the solid residue of [(OEP)Rh<sup>I</sup>]<sup>–</sup>Na<sup>+</sup>. The reaction mixture was stirred at room temperature for 1 h. THF was evaporated and the crude product was chromatographed on an Al<sub>2</sub>O<sub>3</sub> column (6 × 2 cm, type I Basic). The porphyrinic derivative was eluted with a mixture of solvents hexane/toluene (8:2 v/v) [yield 18% based on (OEP)Rh<sup>III</sup>Cl].

**Synthesis of [(TPP)RhIn( $\beta$ -Cl<sub>4</sub>TPP)].** ( $\beta$ -Cl<sub>4</sub>TPP)In<sup>III</sup>Cl (0.04 mmol) was dissolved in 20 mL of THF under an argon atmosphere. The solution was added to the solid residue of [(OEP)Rh<sup>I</sup>]<sup>–</sup>Na<sup>+</sup>. The reaction mixture was stirred at room temperature for 3 h. THF was evaporated and the crude product was passed through an Al<sub>2</sub>O<sub>3</sub> column (5 × 2 cm, type I Basic). The porphyrinic derivative was eluted with toluene [yield 12% based on (TPP)Rh<sup>III</sup>Cl].

- (29) Sadasivan, N.; Fleischer, E. F. *Inorg. Nucl. Chem.* **1968**, *30*, 591.
- (30) (a) Daphnomili, D.; Coutsolelos, A. G. manuscript in preparation. (b) Spyroulias, G. A.; Despotopoulos, A. P.; Raptopoulou, C. P.; Terzis, A.; de Montauzon, D.; Poiblanc, R.; Coutsolelos, A. G. *Inorg. Chem.* **2002**, *124*, 2648

**Table 1.** Crystal Data and Structure Refinement for [(TPP)RhIn(TPyP)]·MeOH

empirical formula	C <sub>85</sub> H <sub>56</sub> N <sub>12</sub> OInRh
fw	1479.19
T (K)	298
wavelength (Å)	Mo K $\alpha$ 0.710730
cryst syst	orthorhombic
space group	F <sub>ddd</sub>
a (Å)	21.52(1)
b (Å)	32.12(2)
c (Å)	20.51(1)
V (Å <sup>3</sup> )	14182(2)
Z	16
d (calcd) (mg/m <sup>3</sup> )	1.385
abs coeff $\mu$ (mm <sup>-1</sup> )	0.615
octants collected	-h, ±k, l
GOF on $F^2$	1.062
final R [ $I > 2\sigma(I)$ ]	0.0821/0.1971 <sup>a</sup>

<sup>a</sup> For 2176 reflections with  $I > 2\sigma(I)$ .

**Synthesis of [(OEP)RhTl( $\beta$ -Cl<sub>8</sub>TPP)].** ( $\beta$ -Cl<sub>8</sub>TPP)Tl<sup>III</sup>·Cl (0.03 mmol) was placed in a Schlenk tube containing 30 mL of dry THF. The solution was added to freshly prepared solid [(OEP)Rh<sup>I</sup>]<sup>-</sup>Na<sup>+</sup> and the mixture was stirred for 2 h at room temperature. The next step was the removal of the solvent under vacuum line followed by the chromatographic separation of the product (Al<sub>2</sub>O<sub>3</sub> column, type I Basic 6 × 2 cm) with a mixture of solvents hexane/toluene (8:2 v/v) as the eluent [15% based on (OEP)Rh<sup>III</sup>Cl].

**X-ray Crystal Structure Determination of [(TPP)RhIn(TPyP)]·MeOH.** A dark red crystal with approximate dimensions 0.20 × 0.20 × 0.30 mm was mounted on a capillary. Diffraction measurements were made on a Crystal Logic dual goniometer diffractometer using graphite monochromated Mo K $\alpha$  radiation. Crystal data and parameters for data collection are reported in Table 1. Unit cell dimensions were determined and refined using the angular settings of 25 automatically centered reflections in the range 11° < 2 $\theta$  < 23°. Intensity data were recorded using a  $\theta$ –2 $\theta$  scan. Three standard reflections monitored every 97 reflections showed <3.0% intensity fluctuation. Lorentz, polarization, and psi-scan absorption corrections were applied using Crystal Logic software. The structure was solved by direct methods using SHELXS-86<sup>31</sup> and refined by full-matrix least-squares techniques on  $F^2$  with SHELXL-93.<sup>32</sup> The structure was solved and refined in the centrosymmetric space group F<sub>ddd</sub>, which required the postulation of disorder for the Rh and In atoms. This model was supported by the presence of a large peak in the Patterson map corresponding to an atom–atom vector of 0.83 Å. The midpoint in the Rh–In bond is the cross section of three mutually perpendicular C<sub>2</sub> axes of symmetry, and as a result, only half of the porphyrinic atoms are crystallographically independent and the Rh and In atoms are 50–50 disordered. Thus, there is no distinction between the tetraphenyl–porphyrin and the tetrapyridyl–porphyrin rings, and their assignment is based on the precursor [(TPP)Rh<sup>III</sup>Cl] and [(TPyP)–In<sup>III</sup>Cl] compounds used for the synthesis of the derivative. Further crystallographic details: 2 $\theta$ <sub>max</sub> = 49°, scan speed 2.2 °/min, scan range 2.3 +  $\alpha_1\alpha_2$  separation, reflections collected/unique/used = 5025/2894 ( $R_{\text{int}} = 0.0602$ )/2894, parameters refined = 237,  $F(000)$  = 6016,  $R1/wR2$  (all data) = 0.1047/0.2147,  $[\Delta\rho]_{\text{max}}/[\Delta\rho]_{\text{min}} = 0.807 / -1.176 \text{ e}/\text{\AA}$ ,  $[\Delta/\sigma] = 0.000$ . All non-hydrogen atoms were refined anisotropically; all hydrogen atoms were introduced at calculated positions as riding on bonded atoms and were refined

isotropically. The carbon atom of the solvent methanol sits on a 2-fold axis of symmetry (site occupancy 0.50). Thus, the oxygen atom is disordered over two positions. The whole molecule was refined isotropically with an occupation factor fixed at 0.25 due to its loss during data collection and no hydrogen atoms were included in the refinement.

**XAS Measurements.** The characterization by XAS spectroscopy of [(OEP)RhIn(OEP)] complex is very delicate because of the rather low yield of the synthesis and of its high photosensitivity,<sup>28</sup> especially at low concentrations.

The spectra for the complex were recorded at the LURE-DCI storage ring (Orsay, France) on XAS 3 experimental station at the rhodium K edge (23 220 eV) and also at indium K edge (27 940 eV) reaching the limits of the DCI incident beam energy. The fluorescence X-ray intensities were detected using the 7 elements Ge-solid Canberra detector, with a positron beam energy of 1.85 GeV and average intensity of 250 mA. On XAS 3 station a Ge(400) double-crystal monochromator was used and no harmonics rejection was needed at such incident beam energies. The microcrystalline powder sample was studied at room temperature in the fluorescence mode, which is efficient for a very dilute metallic sample.<sup>33</sup> Therefore, the experimental spectra were collected in the energy range from 23 100 to 24 100 eV at Rh K edge and in the energy range from 27 800 to 29 000 eV at In K edge, with a 2 eV step, count rate 15 s per point, and with the energy resolution being 2.0 eV. A total of about 8 scans data (about 10 hours per sample) were collected and the absence of the photodegradation of the sample was checked after such a long exposure to beamlight.

**XAS Data Analysis.** The XAS analysis followed a classical method already described.<sup>34</sup> In the fluorescence mode of data collection, the X-ray absorption coefficient is  $\mu(E) = (I_f/I_0)$ , where  $I_0$  and  $I_f$  are the incident and fluorescence beam, respectively. The background contribution  $\mu_b(E)$  was subtracted by a Victoreen function from the experimental spectrum  $\mu(E)$ , whereas the atomic absorption  $\mu_0(E)$  was calculated by an iterative fitting to obtain the EXAFS signal  $\chi(k)$  in k-space. The region of interest of the experimental XAFS signals was filtered in the Fourier transform, with a Kaiser–Bessel window in the range from 1.0 to 11.0 Å<sup>-1</sup> for the Rh–In complex. We used a  $k^2$ -weighting to compensate for the diminishing amplitude at high k, owing to the decay of the photoelectron wave. Then, the obtained XAFS signal was singled out by the back FT procedure in the range 0.5–3.5 Å using a Gaussian window function to include three or four shells using a convenient cutoff which was not complicated by overlapping Fourier transform shells.

Figures 1 and 2 display the XAFS spectra of the bimetallic Rh–In complex at Rh K edge and In K edge, respectively. Noisy EXAFS absorption spectra were observed for both K edges, especially beyond 10 Å<sup>-1</sup>, due to the dilute metallic sample.

For the data collection at the Rh K edge, the modulus of the FT of the Rh–In complex (Figure 1) presents a main peak labeled A at 1.51 Å, with a shoulder B at the downhill at about 2 Å. Also, between 2.5 and 4 Å, a peak C<sub>1</sub>, its shoulder C<sub>2</sub>, and another peak D are observed. Their features indicate that for a quantitative analysis it will be very hard to separate the different peaks that are tightly linked, with probable extension of the indium metal signal on many shells. The peak A and its shoulder B can be assigned to the contribution of the nitrogen atoms of the macrocycle bonded to the rhodium and the indium metals, respectively. The peaks C<sub>1</sub>

(31) Sheldrick, G. M. SHELXS-86, Program for Crystal Structure Solving; University of Gottingen, Germany, 1986.

(32) Sheldrick, G. M. SHELXS-93, Program for Crystal Structure Solving; University of Gottingen, Germany, 1993.

(33) Jacklevic, J.; Kirby, J. A.; Klein, M. P.; Robertson, A. S.; Brown, G. S.; Eisenberger, P. *Solid State Commun.* **1977**, 23, 679.

(34) Agondanou, J. H.; Spyroulias, G. A.; Purans, J.; Tsikalas, G.; Souleau, C.; Coutsolelos, A. G.; Bénazeth, S. *Inorg. Chem.* **2001**, 40, 6088.

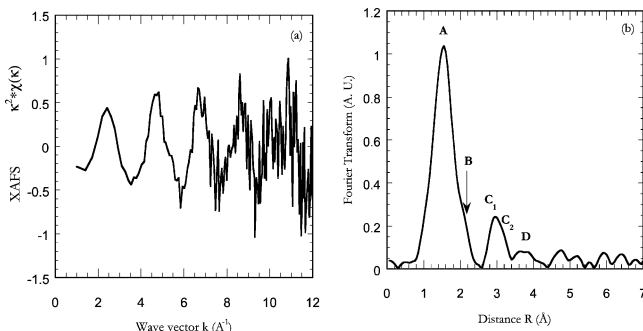


**Figure 1.** (a) Experimental XAFS spectra  $\chi(k)$ .  $k^2$  of Rh–In complex at the Rh K edge, normalized. (b) Experimental FT spectra (modulus part) of Rh–In complex at the Rh K edge (uncorrected from phase shifts).

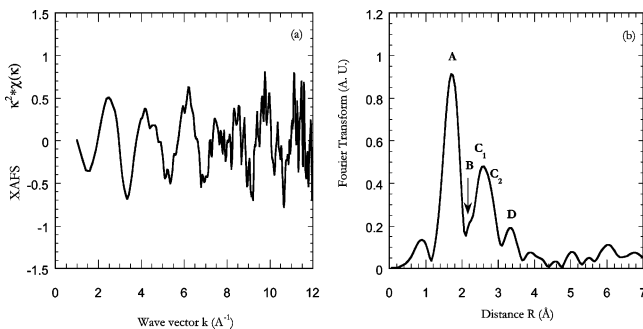


**Figure 2.** (a) Experimental XAFS spectra  $\chi(k)$ .  $k^2$  of the Rh–In complex at In K edge, normalized. (b) Experimental FT spectra (modulus part) of the Rh–In complex at In K edge (uncorrected from phase shifts).

and C<sub>2</sub> correspond to the C <sub>$\alpha$</sub>  and C<sub>meso</sub> carbon atoms of the porphyrinic macrocycle bonded to rhodium. The smaller peak D is strongly damped, due to structural and thermal disorder, and it is almost comparable to noise oscillations. It corresponds to the last C <sub>$\beta$</sub>  carbon atoms of the pyrrole rings, to the ethyl substituents of the porphyrin bonded to the rhodium absorber, and also to the nitrogen atoms of the macrocycle bonded to the indium metal. The carbon atoms from the macrocycle bonded to the indium stand at a long distance, approximately 6 Å further from the absorber, so they cannot interact with the photoelectron or give significant contributions to the signal.

Concerning the In K edge, the resultant FT (Figure 2) presents the same principal peak A, but in this case the rhodium scattering signal seems to have extended on many shells, and its contribution (shoulder B) obviously overlaps with the peaks A and C<sub>1</sub>. This is the origin of the apparent changes observed in the feature of the FT.

After the Fourier transforming step, the fitting procedure was carried out via a classical least-squares algorithm, as developed in the LASE program, which implements the data analysis refinement procedures and offers new tools for error estimation.<sup>35</sup> We allowed the relevant structural parameters to vary: the interatomic distance  $R$  and the Debye–Waller (DW) factor  $\sigma$  which includes both structural and thermal disorders.

The first structural model was built using the X-ray diffraction atomic positions from Wayland et al.<sup>36</sup> With the FEFF6 code<sup>37</sup> we calculated theoretical data for the amplitude and phase functions.

- (35) (a) Curis, E.; Bénazeth, S. *J. Synchrotron Radiat.* **2000**, *7*, 262. (b) Curis, E. <http://www.lure.u-psud.fr/LogicScient/LASE/lase.html>.
- (36) Jones, N. L.; Carroll, P. J.; Wayland, B. B. *Organometallics* **1986**, *5*, 33.
- (37) Rehr, J. J.; Mustre de Leon, J.; Zabinsky, S. I.; Albers, R. C. *J. Am. Chem. Soc.* **1991**, *113*, 5135.

At rhodium and indium K edge, we have carried out EXAFS analyses with a three-shell fit model consisting of the contributions to the signal of the nitrogen atoms, of the transition or nontransition metal (Rh or In), and of C <sub>$\alpha$</sub>  and C<sub>meso</sub> carbon atoms surrounding the photoabsorber. There, indeed, exists an overlap of the various contributions from these atoms which does not allow a separate study on the different shells.

To further investigate the refinement protocol for this Rh–In complex, we also attempted to improve the precision of the determination of distances for the carbon atoms shells by reducing the number of varying parameters. Therefore, we have constrained the Rh–In distance, as the indium atom occupies a strategic position, intermediary between two shells of atoms.

## Results and Discussion

All reactions for the syntheses of the bimetallic complexes were carried out in the dark under strict anaerobic conditions. The formed derivatives are so stable that chromatographic separations can be run in the presence of atmospheric oxygen. They are very sensitive to light.

It must be noted that in the case of the synthesis of dimers, with the participation of tetra- and octahalogenated porphyrin complexes, a slight demetalation of indium porphyrin was observed during the reaction. Similar behavior was observed for the thallium derivatives. This side reaction was expected for Tl porphyrins based on previous results.<sup>28</sup> In this case, both demetalations are probably related to the modification of the redox potential induced by the insertion of Cl atoms in  $\beta$ -pyrrolic positions.<sup>30,38</sup> Also, attempts for the synthesis of heterometallic derivatives with tetrakis-pentafluorophenylporphyrins [(Porph)RhIn(pFTPP)], were not successful at room temperature or at 4 °C. The reason for this may be related to steric hindrance due to the position of pentafluorophenyl groups relative to the porphyrin mean plane,<sup>30a,39</sup> while the powerful electron-withdrawing ability of F atoms cannot be excluded.<sup>40</sup>

The dimetallic complexes are quite stable toward a range of solvents such as PhCH<sub>3</sub>, CH<sub>2</sub>Cl<sub>2</sub>, and THF. In polar solvents, such as DMF and DMSO, they gradually decompose giving the five-coordinated monomer precursors.

**UV/Visible Spectroscopy.** The optical spectra of the studied complexes are characterized by some special features such as the appearance of more than one absorption band in the region of 360–420 nm. In the two series, the insertion of Cl atoms dramatically influences their optical characteristics.

In the case of monomer  $\beta$ -halogenated complexes, a number of papers have reported the influence of two antagonistic effects, the inductive and the distortion, on their optical spectra and on their redox potential.<sup>30b,38,41–44</sup> The distortion of the ring, caused by the halogenation in the

- (38) Bhyrappa, P.; Krishnan, V. *Inorg. Chem.* **1991**, *30*, 239.
- (39) Mandon, D.; Ochsenbein, P.; Fischer, J.; Weiss, R.; Jayaraj, K.; Austin, R. N.; Gold, A.; White, P. S.; Brigaud, O.; Battioni, P.; Mansuy, D. *Inorg. Chem.* **1992**, *31*, 2044.
- (40) (a) Takeuchi, T.; Gray, H. B.; Goddard, W. A. *J. Am. Chem. Soc.* **1994**, *116*, 21, 9730. (b) Hodge, J. A.; Hill, M. G.; Gray, H. B. *Inorg. Chem.* **1995**, *34*, 809.
- (41) D'Souza, F.; Zandler, M. E.; Tagliatesta, P.; Ou, Z.; Shao, J.; Van Caemelbecke, E.; Kadish, K. M. *Inorg. Chem.* **1998**, *37*, 4567.

**Table 2.** UV–Visible Data for the Porphyrinic Dimers [(Porph)RhIn(Porph')] and [(OEP)RhTl(β-Cl<sub>8</sub>TPP)] in Toluene (PhCH<sub>3</sub>)<sup>a</sup>

dimers	B bands			Q bands		
[(OEP)RhIn(TPyP)]	331	<b>369<sup>b</sup></b>	411 (sh)	451	529	603
[(OEP)RhIn(β-Cl <sub>4</sub> TPP)]	324	<b>374<sup>b</sup></b>	418 (sh)	460	531	619
[(OEP)RhIn(β-Cl <sub>8</sub> TPP)]	326	<b>379<sup>b</sup></b>	416 (sh)	474	540	636 (br)
[(OEP)RhTl(β-Cl <sub>8</sub> TPP)]	345	<b>387<sup>b</sup></b>	441 (sh)	460	540	658 (br)
[(TPP)RhIn(TPyP)]	333	379	417 <sup>b</sup>	456	520	594
[(TPP)RhIn(β-Cl <sub>4</sub> TPP)]	338	<b>386<sup>b</sup></b>	418	463	520	611
[(TPP)RhIn(β-Cl <sub>8</sub> TPP)]	340	<b>394<sup>b</sup></b>	434 (sh)	474	525	651 (br) 663

<sup>a</sup>  $\epsilon$  was not measured because of experimental difficulties in handling these compounds. <sup>b</sup> The highest-intensity B band.

$\beta$ -pyrrole position, in conjunction with the electron-withdrawing character of the Cl atoms, modifies the transition energy of the Soret band, and the number and the relative intensities of the Q bands.

Part of this study is to present the influence of  $\beta$ -halogenation in dimetallic porphyrinic complexes. In each of the two series, the ring of the transition metal was kept constant, varying the nontransition metal complexes.

In Table 2, we observe that in the series [(OEP)RhIn-(Porph)] the [(TPyP)In-] unit does not change the  $\lambda_{\max}$  of the Soret band relative to the bimetallic complex [(OEP)-RhIn(TPP)] (370 nm).<sup>27b</sup> The saddle-shape distortion of octahalogenated porphyrin is expected to influence the distance of the two rings and the nature of  $\pi-\pi$  interactions.  $\beta$ -Halogenated porphyrins cause a red shift of the Soret band. Also, a new band between 450 and 500 nm is observed, shifted to lower energy with  $\beta$ -tetra and  $\beta$ -octahalogenated porphyrins, and reaches a 23 nm difference when compared with that of [(TPP)RhIn(TPyP)] derivative (Figure 3).

In the case of [(TPP)RhIn(Porph)] series, the [(TPyP)In-] moiety has no effect on the Soret band related to the complex [(TPP)RhIn(TPP)] (416 nm),<sup>27b</sup> but the  $\lambda_{\max}$  of the Soret band in  $\beta$ -tetra and  $\beta$ -octa halogenated porphyrinic derivatives is gradually blue-shifted: a 23 nm difference in [(TPP)RhIn-( $\beta$ -Cl<sub>8</sub>TPP)] and a 31 nm difference in [TPP)RhIn( $\beta$ -Cl<sub>4</sub>TPP)]. In the B band region for the meso-substituted porphyrins, the higher-intensity B band is observed at 417 nm and the lower-intensity B band is blue-shifted (379 nm).<sup>27</sup> The relative intensities of these two bands are reversed with respect to  $\beta$ -tetrahalogened porphyrins (the higher-intensity band becomes now the lower one), and finally with  $\beta$ -octahalogenated porphyrins the two bands appeared as one broad Soret (Figure 4).

$\beta$ -Halogenated porphyrins also shift the band in the region between 450 and 480 nm. Comparing the position of this band in the series [(OEP)RhIn(Porph)] and [(TPP)RhIn-(Porph)] we observe that this band is independent of the metalloporphyrin moiety of the transition metal, which means that it corresponds to a transition toward an orbital with nontransition metalloporphyrinic character. The band appears at 474 nm for derivatives with  $\beta$ -octahalogenated porphyrins

- (42) Oschenbein, P.; Ayougou, K.; Mandon, D.; Fischer, J.; Weiss, R.; Austin, R. N.; Jayaraj, K.; Gold, A.; Terner, J.; Fajer, J. *Angew. Chem., Int. Ed. Engl.* **1994**, *33*, 3, 348.
- (43) Kadish, K. M.; D'Souza, F.; Villard, A.; Autret, M.; Van Caemelbecke, E.; Bianco, P.; Antonini, A.; Tagliatest, P. *Inorg. Chem.* **1994**, *33*, 23, 5169.
- (44) Spyroulias, A. G.; Despotopoulos, A.; Raptopoulou, C. P.; Terzis, A.; Coutsolelos, A. G. *J. Chem. Soc., Chem. Commun.* **1997**, 783.

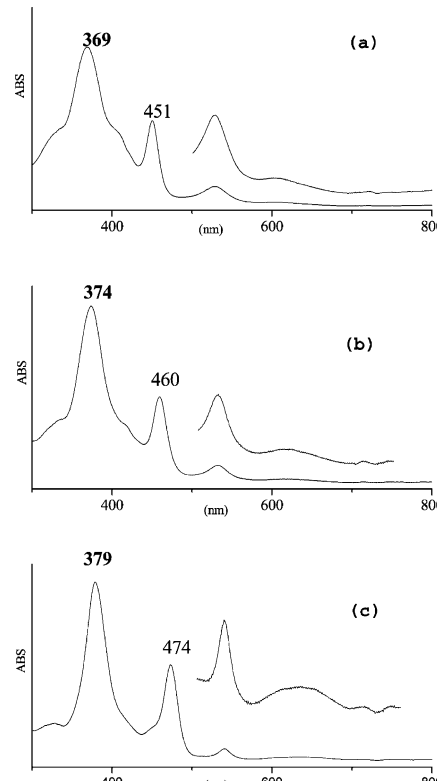


**Figure 3.** UV/Visible spectra of (a) [(OEP)RhIn(TPyP)], (b) [(OEP)RhIn-( $\beta$ -Cl<sub>4</sub>TPP)], and (c) [(OEP)RhIn( $\beta$ -Cl<sub>8</sub>TPP)].

and at 460 nm for the derivatives with  $\beta$ -tetrahalogened porphyrins.

Comparing the optical spectra of [(TPP)RhIn( $\beta$ -Cl<sub>8</sub>TPP)] and [(OEP)RhIn( $\beta$ -Cl<sub>8</sub>TPP)] with that of [(OEP)RhTl( $\beta$ -Cl<sub>8</sub>TPP)] (Figure 5), it can be noticed that this band also depends on the coordination of In or Tl. This is evidence that the orbitals involved in this transition also possess a nontransition metal character. A similar effect is observed for the higher-intensity B band that is blue-shifted for the more electronegative Tl atom. Theoretical studies on monomer complexes have revealed a correlation between the electronegativity of the metal and the energies of HOMO orbitals.<sup>45</sup>

Consequently, in both series, halogenated porphyrins influence the nature of the  $\pi-\pi$  interactions. The effect is differentiated for the higher-intensity B band (as expressed by the  $\lambda_{\max}$  shifts) by the nature of the macrocycle (OEP, TPP) of the transition metal. Also characteristic is the new band between 450 and 480 nm, which possesses a charge

- (45) Shelton, J. A.; Ortiz, V. *J. Phys. Chem.* **1985**, *89*, 4733.

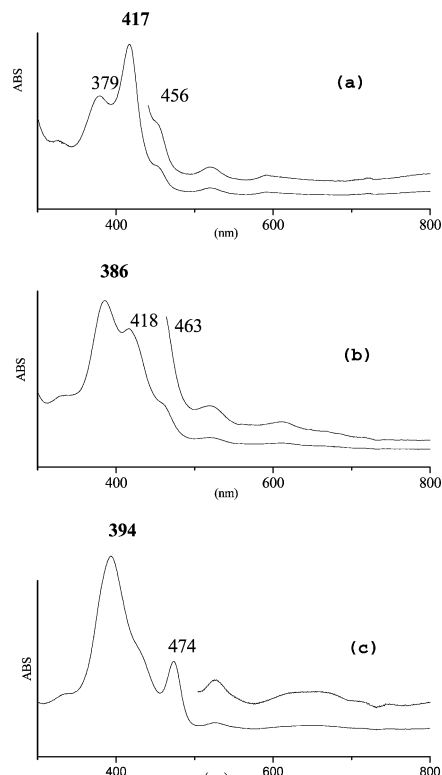


**Figure 4.** UV/Visible spectra of the dimers (a)  $[(\text{TPP})\text{RhIn}(\text{TPyP})]$ , (b)  $[(\text{TPP})\text{RhIn}(\beta\text{-Cl}_4\text{TPP})]$ , and (c)  $[(\text{TPP})\text{RhIn}(\beta\text{-Cl}_8\text{TPP})]$ .

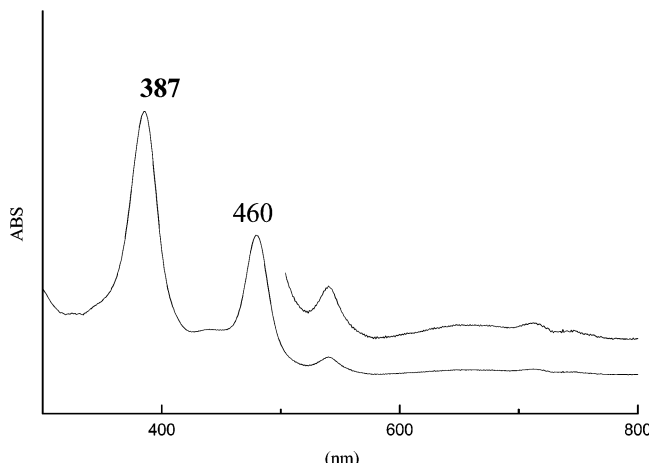


**Figure 5.** UV/Visible spectrum of  $[(\text{OEP})\text{RhTl}(\beta\text{-Cl}_8\text{TPP})]$ .

transfer character depending only on the nontransition metalloporphyrin.

**NMR Studies.** The chemical shifts for the synthesized derivatives are presented in Table 3. For the assignment of each signal to a specific proton several NMR experiments were performed: 2D-COSY, TOCSY, HMQC, and HMBC in addition to the  $^1\text{H}$  and  $^{13}\text{C}$  NMR spectra.

Generally the bimetallic porphyrinic system creates shielding and deshielding regions with the most important centers being the dimetallic bond and the current of the porphyrin ring. The presence of the two macrocyclic ligands substantially affects the magnetic field experienced by the protons.

In the series of bimetallic complexes with one OEP ring, the  $^1\text{H}$  NMR spectra can be interpreted on the basis of two

distinct regions: the aliphatic region for the ethyl group of  $[(\text{OEP})\text{Rh-}]$  part and the phenyl region for the  $[(\text{Porph})\text{In-}]$  part of the bimetallic derivatives. The meso-H are upfield shifted with the most shielded ones being those of complex  $[(\text{OEP})\text{RhIn}(\text{TPyP})]$ . As far as the phenyl protons, ortho-exo ( $\text{o}'\text{-H}$ ), meta-exo ( $\text{m}'\text{-H}$ ), and pyr-H are upfield shifted. In contrast, the ortho-endo ( $\text{o-H}$ ) and meta-endo ( $\text{m-H}$ ) are shifted downfield. The highest values of shielding and deshielding effects are observed for the  $\text{o-H}$  and  $\text{o}'\text{-H}$  of complex  $[(\text{OEP})\text{RhIn}(\beta\text{-Cl}_4\text{TPP})]$ .

Comparing the chemical shifts of  $[(\text{OEP})\text{RhIn}(\beta\text{-Cl}_8\text{TPP})]$  and  $[(\text{OEP})\text{RhTl}(\beta\text{-Cl}_8\text{TPP})]$ , we deduced that the ring current effects are more pronounced in the former complex. A possible explanation for the above observation could be given if we consider the ionic radii of the two nontransition metals as well as their position, out of the porphyrin plane.<sup>30a</sup> For  $[(\text{OEP})\text{RhTl}(\beta\text{-Cl}_8\text{TPP})]$ , a larger distance of the two rings is expected and consequently a reduced current of the two porphyrinic rings.

For the derivatives with two tetraphenyl porphyrinic rings, the chemical shift of the protons is observed in a range of approximately 2 ppm.

Concerning the  $[(\text{TPP})\text{RhIn}(\text{TPyP})]$  derivative, the presence of the phenyl groups presents two difficulties: the identification of each signal for a specific proton and then the assignment of that proton to the corresponding porphyrin ring. In the 2D-COSY spectrum (Figure 6a), a correlation can be observed between the H at 7.20 ppm and that at 7.48 ppm. These signals are attributed to  $\text{o}'\text{-H}$  and  $\text{m}'\text{-H}$  protons of the  $[(\text{TPP})\text{Rh-}]$  moiety. The  $\text{m}'\text{-H}$  appears as a triplet in the  $^1\text{H}$  NMR due to coupling with the  $p\text{-H}$  protons. From the couplings of  $p\text{-H}$ , the triplet at 7.94 ppm is attributed to  $\text{m-H}$  and the doublet at 8.75 ppm is attributed to  $\text{o-H}$  protons of the phenyl ring of the  $[(\text{TPP})\text{Rh-}]$  part in the derivative. Some of the phenyl protons of the  $[(\text{TPyP})\text{In-}]$  moiety give broad bands in the  $^1\text{H}$  NMR spectra of equal intensities, due to the flipping motion of the ring,<sup>46</sup> and one proton resonance at the same field with the  $\text{o-H}$  protons of the  $[(\text{TPP})\text{Rh-}]$  moiety. The spin network of the  $[(\text{TPyP})\text{In-}]$  was observed on TOCSY experiments (Figure 6b), where  $\text{m-H}$  (9.22 ppm) was coupled through magnetization transfer to  $\text{o-H}$ ,  $\text{o}'\text{-H}$ , and  $\text{m}'\text{-H}$  protons.

In an analogous way, the characterization of  $[(\text{TPP})\text{RhIn}(\beta\text{-Cl}_8\text{TPP})]$  protons was achieved. Although the chemical shifts of the corresponding monomers differ significantly,<sup>30a</sup> the formation of the dimetallic complex causes modifications such that all the protons resonate in a range of 1.5 ppm. Some phenyl protons of the two rings resonate at the same field, as judged by the intensities of  $^1\text{H}$  NMR signals. The combination of 2D-COSY, HMQC, and HMBC experiments led to the unambiguous assignment of the  $^1\text{H}$  NMR spectrum. The  $^{13}\text{C}$  NMR chemical shifts were assigned through heteronuclear experiments, Table 4. For the  $[(\text{OEP})\text{RhTl}(\beta\text{-Cl}_8\text{TPP})]$  complex,  $\text{C}_\beta$  carbon of the octachloro ring is

(46) (a) Eaton, S. S.; Eaton, C. R. *J. Am. Chem. Soc.* **1977**, *97*, 3660. (b) Davoras, E. M.; Spyroulias, G. A.; Mikros, E.; Coutsolelos, A. G. *Inorg. Chem.* **1997**, *33*, 3430.

**Table 3.**  $^1\text{H}$  NMR Data for [(Porph)RhIn(Porph')] and [(OEP)RhTl( $\beta$ -Cl<sub>8</sub>TPP)] Complexes in CDCl<sub>3</sub>

	tetra-aryl porphyrin ring <sup>a</sup>						(OEP) ring		
	(o-H)	(o'-H)	(m-H)	(m'-H)	(p-H)	(pyr-H)	meso-H	CH <sub>2</sub>	CH <sub>3</sub>
[(TPP)Rh-In(TPyP)]	8.75 (d) 8.98 (s,br)	7.20 (d) 7.07 (s,br)	7.94 (m) 9.22 (s,br)	7.48 (m) 8.75 (d)	7.78 (tr)	8.21 (s) 8.52 (s)			
[(TPP)Rh-In( $\beta$ -Cl <sub>8</sub> TPP)]	8.50 (d) 8.76 (d)	7.04 (d) 7.04 (d)	7.80 (m) 7.96 (m)	7.41 (m) 7.41 (m)	7.71 (tr) 7.73 (tr)	8.40 (s)			
[(TPP)Rh-In( $\beta$ -Cl <sub>4</sub> TPP)]	8.73 (d) 8.81 (d)	7.23 (d) 6.87 (d)	8.24 (m) 8.26 (m)	7.47 (m) 7.47 (m)	7.75 (tr) 7.75 (tr)	8.27 (s) 8.31 (s)			
[(OEP)Rh-In(TPyP)]							8.71 (s)	4.02/ 3.79 (m)	1.53 (tr)
[(OEP)Rh-In( $\beta$ -Cl <sub>8</sub> TPP)]	9.21 (s,br)	6.99 (s,br)	9.52 (s,br)	8.71 (d)		8.76 (s)	9.2 (s)	4.13/ 3.77 (m)	1.51 (tr)
[(OEP)Rh-In( $\beta$ -Cl <sub>4</sub> TPP)]	8.93 (d)	7.17 (d)	8.19 (m)	7.48 (m)	7.86 (tr)		9.2 (s)	4.19/ 3.85 (m)	1.53 (tr)
[(OEP)Rh-Tl( $\beta$ -Cl <sub>8</sub> TPP)]	9.17 (d)	6.65 (d)	8.19 (m)	7.33 (m)	7.78 (tr)	8.97 (s)	9.48 (s)	4.20/ 3.82 (m)	1.59 (tr)
	8.66 (d)	7.31 (d)	8.16 (m)	7.50 (m)	7.85 (tr)				

<sup>a</sup> The hydrogen atoms defined as ortho (*o*), ortho-endo; ortho' (*o'*), ortho-exo; meta (*m*), meta-endo; meta' (*m'*), meta-exo.

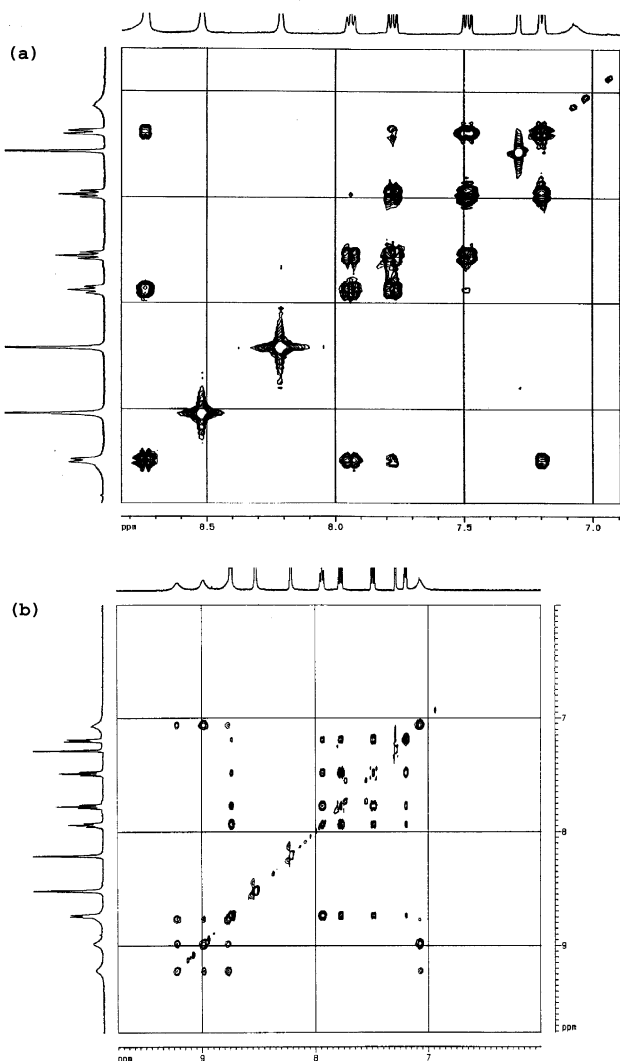


**Figure 6.** (a) 2D COSY spectrum of [(TPP)RhIn(TPyP)], and (b) TOCSY spectrum of [(TPP)RhIn(TPyP)].

considerably shifted (131.70 ppm) compared to the chemical shift of the corresponding monomer (137.8 ppm).<sup>30a</sup> This fact is related to the formation of the dimer, accompanied with

a different chemical environment and/or with a possible change of the relative peak positions.

**Crystal Structure of [(TPP)RhIn(TPyP)].** The structure consists of a rhodium tetraphenylporphyrin group and an indium tetrapyridylporphyrin group joined facially by a bond. The two porphyrin rings, defined by the two C<sub>20</sub>N<sub>4</sub> cores, are parallel to each other as required by the symmetry elements. The ORTEP diagram of the molecular structure of [(TPP)RhIn(TPyP)] and the deviations of the crystallographically independent porphyrin atoms from the C<sub>20</sub>N<sub>4</sub> mean plane are given in Figure 7, while a side view of the derivative is given in Figure 8. Selected bond distances and angles are given in Table 5. The [(TPP)Rh-] moiety is twisted by ca. 35° with respect to the [(TPyP)In-] moiety (the twist angle is defined as the average of the N<sub>x</sub>–Rh–In–N<sub>x</sub> (*x* = 1–4) torsion angles).

The two metal atoms are displaced from the plane of the four coordinated pyrrole nitrogen atoms toward each other (0.04 Å for Rh and 0.87 Å for In). These values are comparable to those observed in the analogous derivative compound [(OEP)RhIn(OEP)]<sup>36</sup> (0.01 Å for Rh and 0.83 Å for In) as well as those found in the monomer compounds [(TPP)In<sup>III</sup>(CH<sub>3</sub>)]<sup>47</sup> (0.78 Å) and [(OEP)Rh<sup>III</sup>(CH<sub>3</sub>)]<sup>48</sup> (0.05 Å). The presence of the metal ions in the porphyrin cavity, in combination with the phenyl substituents on the C<sub>meso</sub> atoms, was responsible for the twist distortion of the porphyrin skeleton. The average deviation of the C<sub>meso</sub> atoms from the C<sub>20</sub>N<sub>4</sub> mean plane is 0.095 Å. The phenyl rings are rotated by ca. 55 and 71° (for the phenyls defined by C<sub>11</sub>–C<sub>16</sub> and C<sub>17</sub>–C<sub>22</sub>, respectively) with respect to the C<sub>20</sub>N<sub>4</sub> mean plane.

The Rh–N distances (average 2.042 Å) are very similar to those reported for [(OEP)Rh<sup>III</sup>(CH<sub>3</sub>)] (2.031 Å), [(OEP)Rh<sup>III</sup>(CHO)] (2.03 Å), and [(OEP)Rh<sup>III</sup>H] (2.02 Å). The In–N distances (average 2.220 Å) are comparable to those found

(47) Lecomte, C.; Protas, J.; Cocolios, P.; Guilard, R. *Acta Crystallogr. B*. **1980**, *B36*, 2769.

(48) Takenaka, A.; Syal, S. K.; Sasada, Y.; Omura, T.; Ogoshi, H.; Yoshida, Z.-I. *Acta Crystallogr. B*. **1976**, *B32*, 62.

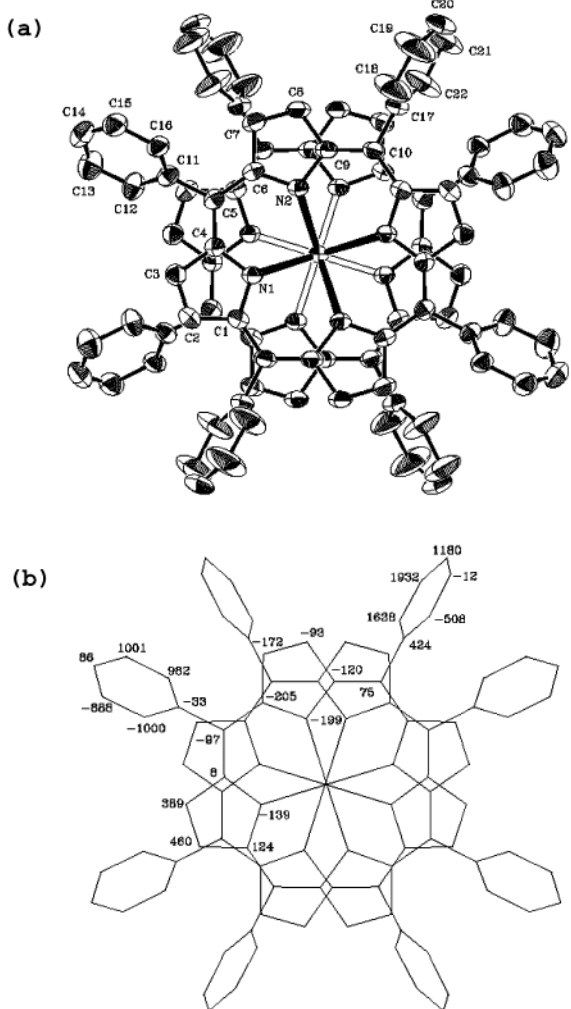


**Figure 7.** (a) ORTEP diagram of the  $[(\text{TPP})\text{RhIn}(\text{TPyP})]$  looking down the Rh–In bond, showing the labeling of the crystallographically independent porphyrin atoms (thermal ellipsoids have been drawn at the 30% probability level). Hydrogen atoms have been omitted for clarity. (b) Displacements ( $\times 10^3 \text{ \AA}$ ) of the crystallographically independent porphyrin atoms of the  $\text{C}_{20}\text{N}_4$  mean plane.

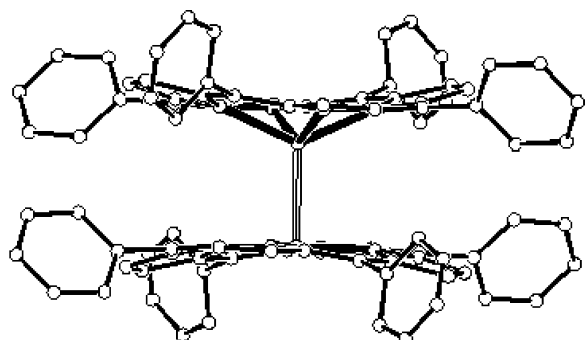


**Figure 8.** Side view of the  $[(\text{TPP})\text{RhIn}(\text{TPyP})]$ .

in  $[(\text{TPP})\text{In}^{\text{III}}(\text{CH}_3)]$  ( $2.20 \text{ \AA}$ ) and longer than those found in  $[(\text{OEP})\text{In}^{\text{III}}(\text{O}_2\text{CCH}_3)]$  ( $2.125 \text{ \AA}$ ). This is due to the larger deviation of the indium atom from the  $\text{N}_4$  plane ( $0.83 \text{ \AA}$  in  $\text{In}(\text{TPyP})$  and  $0.61 \text{ \AA}$  in  $\text{In}(\text{OEP})$ ). Finally, the metal–nitrogen distances in  $[(\text{TPP})\text{RhIn}(\text{TPyP})]$  are similar to those found in  $[(\text{OEP})\text{RhIn}(\text{OEP})]$ <sup>36</sup> (average values  $\text{Rh–N} = 2.036$  and  $\text{In–N} = 2.202 \text{ \AA}$ ). The Rh–In bond length of

**Table 4.**  $^{13}\text{C}$  NMR Data of  $[(\text{Porph})\text{RhIn}(\text{Porph}')]$  and  $[(\text{OEP})\text{RhIn}(\beta\text{-Cl}_8\text{TPP})]$  in  $\text{CDCl}_3^a$

	$[(\text{TPP})\text{RhIn-}(\text{TPyP})]$	$[(\text{TPP})\text{RhIn-}(\beta\text{-Cl}_8\text{TPP})]$	$[(\text{OEP})\text{RhIn-}(\text{TPyP})]$
$\text{C}_o$	133.82/127.17	135.21/133.16	130.99
$\text{C}_{o'}$	135.83/130.55	135.58/135.70	131.89
$\text{C}_m$	126.70/148.53	127.20/127.85	148.33
$\text{C}_{m'}$	127.17/148.35	127.05/128.17	148.33
$\text{C}_{\text{para}}$	127.88	129.21/128.17	
$\text{C}_{\text{ph}}$	141.82/148.12	141.28/137.90	148.12
$\text{C}_{\alpha}$	142.53/150.09	142.21/151.9	139.59/150.48
$\text{C}_{\beta}$	130.83/131.27	131.70/134	140.13/131.26
$\text{C}_{\text{meso}}$	120.80/118.12	120.21/121.56	98.49/119.37
$\text{CH}_2$			20.55
$\text{CH}_3$			18.35
	$[(\text{OEP})\text{RhIn-}(\beta\text{-Cl}_8\text{TPP})]$	$[(\text{OEP})\text{RhIn-}(\beta\text{-Cl}_8\text{TPP})]$	$[(\text{OEP})\text{RhTl-}(\beta\text{-Cl}_8\text{TPP})]$
$\text{C}_o$	135.58	133.71	135.42
$\text{C}_{o'}$	136.02	135.01	135.87
$\text{C}_m$	127.92	126.18	128.09
$\text{C}_{m'}$	128.21	127.36	127.85
$\text{C}_{\text{para}}$	129.28	128.27	129.16
$\text{C}_{\text{ph}}$	141.20	141.14	138.61
$\text{C}_{\alpha}$		140.29/140.99	142.14
$\text{C}_{\beta}$	132.20	134.35/135.35	141.83/131.70
$\text{C}_{\text{meso}}$	98.76/121.77	98.52	99.17/119.82
$\text{CH}_2$	20.55	20.71	20.55
$\text{CH}_3$	18.35	18.32	18.33

<sup>a</sup> The carbon atoms defined as ortho (*o*), ortho-endo; ortho' (*o'*), ortho-exo; meta (*m*), meta-endo; meta' (*m'*), meta-exo.

**Table 5.** Selected Bond Distances ( $\text{\AA}$ ) and Angles ( $^\circ$ ) for  $[(\text{TPP})\text{RhIn}(\text{TPyP})]\cdot\text{MeOH}$

Distances			
Rh–In	2.545(3)	In–N1	2.224(5)
Rh–N( <i>1<sup>a</sup></i> )	2.036(5)	In–N(2)	2.216(5)
Rh–N( <i>2<sup>a</sup></i> )	2.048(5)	In–N( <i>1<sup>c</sup></i> )	2.224(5)
Rh–N( <i>1<sup>b</sup></i> )	2.036(5)	In–N( <i>2<sup>c</sup></i> )	2.216(5)
Rh–N( <i>2<sup>b</sup></i> )	2.048(5)		
Angles			
N( <i>1<sup>a</sup></i> )–Rh–N( <i>2<sup>a</sup></i> )	89.5(2)	N( <i>1<sup>a</sup></i> )–In–N(2)	80.7(2)
N( <i>1<sup>a</sup></i> )–Rh–N( <i>1<sup>b</sup></i> )	176.4(3)	N( <i>1<sup>a</sup></i> )–In–N( <i>1<sup>c</sup></i> )	132.4(3)
N( <i>1<sup>a</sup></i> )–Rh–N( <i>2<sup>b</sup></i> )	90.5(2)	N( <i>1<sup>a</sup></i> )–In–N( <i>2<sup>c</sup></i> )	81.5(2)
N( <i>2<sup>a</sup></i> )–Rh–N( <i>1<sup>b</sup></i> )	90.5(2)	N( <i>2<sup>a</sup></i> )–In–N( <i>1<sup>c</sup></i> )	81.5(2)
N( <i>2<sup>a</sup></i> )–Rh–N( <i>2<sup>b</sup></i> )	179.2(3)	N( <i>2<sup>a</sup></i> )–In–N( <i>2<sup>c</sup></i> )	135.1(3)
N( <i>1<sup>b</sup></i> )–Rh–N( <i>2<sup>b</sup></i> )	89.5(2)	N( <i>1<sup>c</sup></i> )–In–N( <i>2<sup>c</sup></i> )	80.7(2)

<sup>a</sup>  $0.25 - x$ ,  $0.25 - y$ ,  $z$ . <sup>b</sup>  $x$ ,  $0.25 - y$ ,  $0.25 - z$ . <sup>c</sup>  $0.25 - x$ ,  $y$ ,  $0.25 - z$ .

$2.545(3) \text{ \AA}$  is not significantly different from the value estimated for a Rh–In single bond ( $2.62 \text{ \AA}$ ), similar to that found in  $[(\text{OEP})\text{RhIn}(\text{OEP})]$  ( $2.584(2) \text{ \AA}$ ), and shorter than the multiple bond between transition metals.<sup>16–17,19</sup>

**EXAFS.** The structural modeling for the Rh–In complex was performed in the range  $4–11 \text{ \AA}^{-1}$ , on a filtered spectrum including the first three peaks of the FT at both Rh and In K edges. The first three peaks (A, C<sub>1</sub>, and C<sub>2</sub>) are mainly influenced by single scattering processes, even though in the third peak (C<sub>2</sub>) some multiple scattering processes may appear. In this fitting procedure, we had to take into account that the contribution of the heavy indium metal is likely to interfere with contributions at higher distances.

**Rh K Edge of the Bimetallic  $[(\text{OEP})\text{RhIn}(\text{OEP})]$ .** For the best-fit analysis at the Rh K edge, we have considered a number of independent points  $N_{\text{ind}} = 9$  ( $\Delta k = 7 \text{ \AA}^{-1}$  and  $\Delta R = 3 \text{ \AA}$ ). The fitting results on the EXAFS filtered spectrum are gathered in Table 6. The values found for the

**Table 6.** Structural Data Obtained from the Best-Fit Analysis of the Rh–In Complex at the Rh K Edge<sup>a</sup>

bond	(EXAFS)			(XRD) <sub>1</sub>	(XRD) <sub>2</sub>	
	<i>N</i> <sub>1</sub>	<i>R</i> <sub>1</sub> (Å)	$\sigma_1^2$ (Å <sup>2</sup> )	$\epsilon_1$ ( $\times 10^3$ )	<i>R</i> <sub>2</sub> (Å)	<i>R</i> <sub>2</sub> (Å)
Rh–N	4	2.029	0.004	5.6	2.036	2.042
Rh–In	1	2.578	0.005		2.584	2.545
Rh–C <sub>α</sub>	8	3.021	0.007		3.062	
Rh–C <sub>meso</sub>	4	3.418	0.005		3.401	

<sup>a</sup> *N* (not fitted parameter) is the number of atoms located in the various shells at the distance *R* from the Rh absorber,  $\sigma^2$  is the DW factor, and  $\epsilon$  is the fitting error. (XRD)<sub>1</sub> and (XRD)<sub>2</sub> represent the X-ray diffraction data of the bimetallic complexes [(OEP)RhIn(OEP)] and [(TPP)RhIn(TPyP)], respectively.

two distances Rh–N = 2.029 ± 0.010 Å and Rh–In = 2.578 ± 0.010 Å (from the peak A and shoulder B) are still in good agreement with the X-ray data of 2.036 and 2.584 Å, respectively, for the same complex. The difference between the two techniques (X-ray and XAS) for these bond lengths is of the order of 0.006 Å, which is excellent. The replacement of the (OEP) ligand by (TPP) and (TPyP) ligands slightly modifies the Rh–N and Rh–In bond lengths, with X-ray values of 2.042 and 2.545 Å, respectively, for the bimetallic [(TPP)RhIn(TPyP)]. These distance values are quite comparable with those of the Rh–In bis-octaethylporphyrinate.

Concerning the values of the Rh–C<sub>α</sub> and Rh–C<sub>meso</sub> bond distances, they are found to be shorter than expected. Actually, with this filtered spectrum the mean distances are as follows: Rh–C<sub>α</sub> = 3.021 ± 0.020 Å and Rh–C<sub>meso</sub> = 3.418 ± 0.020 Å (from the peaks C<sub>1</sub> and C<sub>2</sub>). These values slightly differ from the calculated crystallographic values of 3.062 and 3.401 Å, respectively. However, a gap of 0.03 Å between the two techniques is reasonable, knowing that XAS spectroscopy has the tendency to give slightly shorter distances than the ones determined by XRD. This difference is partly due to approximations in the theory, coupled with the lack of resolution at similar distances.<sup>49</sup>

In the case of a fitting procedure with constraints on the Rh–N and Rh–In distances, the improvement in the results for the carbon atoms is clearly visible in the DW factors and distances. For instance, the distances for the carbon atoms are increased, thus being much closer to the X-ray data, and the DW factors values are lowered.

**In K Edge of the Bimetallic [(OEP)RhIn(OEP)].** At the In K edge, the fitting results obtained for the [(OEP)RhIn(OEP)] complex are listed in Table 7. The obtained values reflect a reasonable In–Rh distance, identical to the distance found at Rh K edge. The EXAFS value is still in quite good agreement with the X-ray value, with a difference of only 0.005 Å for this bond length. Nevertheless, in all our simulations, the distance between the absorber indium and the nitrogen atoms is fixed at 2.16 Å, which means that it is

(49) Binsted, N.; Strange, R. W.; Hasnain, S. S. *Biochemistry* **1992**, *31*, 12117.

**Table 7.** Structural Data Obtained from the Best-Fit Analysis of the Rh–In Complex at the In K Edge<sup>a</sup>

bond	(EXAFS)			(XRD) <sub>1</sub>	(XRD) <sub>2</sub>	
	<i>N</i> <sub>1</sub>	<i>R</i> <sub>1</sub> (Å)	$\sigma_1^2$ (Å <sup>2</sup> )	$\epsilon_1$ ( $\times 10^3$ )	<i>R</i> <sub>2</sub> (Å)	<i>R</i> <sub>2</sub> (Å)
In–N	4	2.163	0.004	7.3	2.203	2.220
In–Rh	1	2.581	0.003		2.584	2.545
In–C <sub>α</sub>	8	3.134	0.008		3.161	
In–C <sub>meso</sub>	4	3.456	0.004		3.461	

<sup>a</sup> *N* (not fitted parameter) is the number of atoms located in the different shells at a distance *R* from the In metal,  $\sigma^2$  is the DW factor,  $\epsilon$  is the fitting error. (XRD)<sub>1</sub> and (XRD)<sub>2</sub> represent the X-ray diffraction data of the bimetallic complexes [(OEP)RhIn(OEP)] and [(TPP)RhIn(TPyP)], respectively.

shorter than the one determined by XRD (In–N = 2.20 Å for the bimetallic [(OEP)RhIn(OEP)] and 2.22 Å for the [(TPP)RhIn(TPyP)] complex). The difference between the two techniques is not too strong within experimental error margins and we must emphasize that this distance value given by X-ray is the longest ever found for an indium–nitrogen bond length in a square pyramidal conformation.<sup>36,50</sup>

## Conclusions

The new series of presented derivatives with Rh–In bonds exhibit interesting optical features which are monitored by the number and the position of the peripheral substitution. Also, a key role is played by the nature of the nontransition metal as judged by the comparison of derivatives containing In or Tl as central metal. The X-ray structure of [(TPP)RhIn(TPyP)] shows a length of single bond of 2.545 Å. XAS spectroscopy on the Rh–In bimetallic complex has provided a consistent determination of the distance of 2.58 Å, at both Rh and In K edges, very similar to the X-ray data. XAS spectroscopy investigation of the more distant carbon atom shells has also given accurate results, while reducing the number of independent points in the data treatment.

The determination of metal–metal bond length for the titled complexes was performed by two different approaches. XAS and X-ray techniques provide similar data and this fact could be used for future structural determinations on powder samples.

**Acknowledgment.** This research was supported by the Greek General Secretariat of Research and Technology, and the EPEAEK graduate programs of “Bionorganic Chemistry” and “Natural Products” through the Special Research Account of the University of Crete.

**Supporting Information Available:** Listings of crystal structure refinement data, positional and thermal parameters, and bond distances and angles. HMQC and HMBC spectra of [(TPP)RhIn( $\beta$ -Cl<sub>8</sub>TPP)] in CDCl<sub>3</sub> and <sup>1</sup>H NMR spectrum of [(TPP)RhIn(TPyP)] in CDCl<sub>3</sub> (pdf). This material is available free of charge via the Internet at <http://pubs.acs.org>.

IC035155X

(50) Robinson, W. R.; Schussler, D. P. *Inorg. Chem.* **1973**, *12*, 848.